

RESEARCH ARTICLE

10.1002/2015JF003789

Key Points:

- Details of glacier runoff module addition to existing hydrological simulation code (Precipitation Runoff Modeling System (PRMS))
- Module designed to work in remote areas with works with limited or no on-glacier measurements
- Module tested on two well-studied glaciers and showed comparable results to other models with more data and computation demands

Correspondence to:

A. E. Van Beusekom,
beusekom@usgs.gov

Citation:

Van Beusekom, A. E., and R. J. Viger (2016), A glacier runoff extension to the Precipitation Runoff Modeling System, *J. Geophys. Res. Earth Surf.*, 121, 2001–2021, doi:10.1002/2015JF003789.

Received 13 NOV 2015

Accepted 7 OCT 2016

Accepted article online 17 OCT 2016

Published online 4 NOV 2016

Published [2016]. This article is a US Government work and is in the public domain in the USA.

A glacier runoff extension to the Precipitation Runoff Modeling System

A. E. Van Beusekom¹ and R. J. Viger²

¹USDA Forest Service International Institute of Tropical Forestry, Río Piedras, Puerto Rico, ²United States Geological Survey, Denver, Colorado, USA

Abstract A module to simulate glacier runoff, PRMSGlacier, was added to PRMS (Precipitation Runoff Modeling System), a distributed-parameter, physical-process hydrological simulation code. The extension does not require extensive on-glacier measurements or computational expense but still relies on physical principles over empirical relations as much as is feasible while maintaining model usability. PRMSGlacier is validated on two basins in Alaska, Wolverine, and Gulkana Glacier basin, which have been studied since 1966 and have a substantial amount of data with which to test model performance over a long period of time covering a wide range of climatic and hydrologic conditions. When error in field measurements is considered, the Nash-Sutcliffe efficiencies of streamflow are 0.87 and 0.86, the absolute bias fractions of the winter mass balance simulations are 0.10 and 0.08, and the absolute bias fractions of the summer mass balances are 0.01 and 0.03, all computed over 42 years for the Wolverine and Gulkana Glacier basins, respectively. Without taking into account measurement error, the values are still within the range achieved by the more computationally expensive codes tested over shorter time periods.

1. Introduction

When simulating the hydrology of basins containing glaciers, explicitly representing the dynamics of the glaciated landscape and its interaction with the nonglaciated surfaces is critical to accurately simulate the hydrology of regional-sized basins [Clarke *et al.*, 2015]. In addition to assessing the impacts of climate change on glacier and general hydrologic response, this type of integrated modeling is important for societies that need to manage water resources. Although there are a number of detailed physical models of glacier hydrology, they tend to be standalone products that when integrated with more general hydrological models are so complex and have such extensive input data needs that their usability is substantially reduced [Li *et al.*, 2015]. In addition, the temporal and spatial scale of historically available glacier data has been so poor as to create a further obstacle to representing glaciers (well) in general physically based hydrological simulations.

This manuscript builds on previous contributions to the literature, developing and demonstrating an implementation of a module to simulate glacier dynamics that has been added to an existing hydrological distributed-parameter, physical-process simulation code, Precipitation Runoff Modeling System (PRMS) [Leavesley *et al.*, 1983; Markstrom *et al.*, 2015]. The demonstration will be made by application of PRMSGlacier to two basins in southern Alaska, which contain the Wolverine and Gulkana glaciers. This work contributes a broadly usable approach for integrating glacier dynamics into hydrologic simulation that balances the physical realism of a model with its usability.

2. Past Studies

There is a relative scarcity of quantitative modeling studies that define a framework for evaluating the flow characteristics of regional-scale glacier-driven basins [Huss, 2011; Nolin *et al.*, 2010; Radić and Hock, 2014]. Most glacier-simulation studies found in the literature focus on small basins (10–200 km² [e.g., Farinotti *et al.*, 2012; Grossi *et al.*, 2013]), which do not focus on interaction of the currently glacier-covered (glacierized) and unglacierized land that is critical to modeling regional-sized basins. Detailed on-glacier input data are used in these studies that make the effort of setting up regional applications prohibitive [e.g., Immerzeel *et al.*, 2012; Shea *et al.*, 2015]. On the other extreme, global land models make use of continental-scale ice models [e.g., Lipscomb *et al.*, 2013; Rutt *et al.*, 2009] that are not designed to explore specific regions or to make calculation on daily time steps. The regional application codes that are available demand large amounts of very accurate input data, such as detailed glacier basal topography [e.g., Clarke *et al.*, 2015; Naz

et al., 2014], and detailed weather data such as wind, radiation, and humidity [e.g., *Naz et al.*, 2014; *Ragetti and Pellicciotti*, 2012], which are not widely available. Researchers have recognized that lack of quality data is a problem in inclement and typically remote glacierized areas. Even glacier models that have fewer data requirements [such as *Li et al.*, 2015] still require glacier thickness estimates.

Hydrologic models that simulate glacial melt contribution to overall streamflow discharge in Alaska have been published, but these studies focused on delivery of freshwater into coastal systems for oceanic modeling, and thus contained relatively simplistic representations of glacier and hydrological dynamics [e.g., *Royer*, 1982; *Wang et al.*, 2004]. Because of the general modeling frameworks used, these studies provide estimates of seasonal contributions rather than simulations of glacier physics [*Hill et al.*, 2015]. Other authors have integrated Alaskan glacier volume loss estimates in their regional estimates (such as *Hill et al.* [2015] and *Neal et al.* [2010]), but these are lumped estimates for each basin that are based on regression-based estimates of hydrology. Although several of these modeling efforts do include Alaskan glacier volume loss estimates through time, many use relations based on statistics or empirically derived coefficients. The few studies that have physically represented glaciers in Alaska tend to use simplistic representations for the rest of the terrestrial hydrologic cycle or lack discretization of subbasin features [e.g., *Bliss et al.*, 2014].

3. Study Areas

Two basins will be used to demonstrate PRMSGlacier. These are the basins that contain the Gulkana and Wolverine glaciers. Both basins are located in Alaska (Figure 1), are of similar size and aspect (southerly), and contain glaciers whose behavior is a substantial contributor to the overall streamflow regime [*O'Neel et al.*, 2014]. However, these basins have contrasting climatic conditions and therefore provide a range of glacier behavior. Each basin's climate, streamflow, and glacier mass balance (MB) (glacier-wide thickness change in meter water equivalent) has been extensively monitored since 1966 by the United States Geological Survey (USGS), as part of a "benchmark glacier" system representative of regional glacier-climate interactions. This helps provide the data necessary to assess the performance of the glacier-enhanced model simulation.

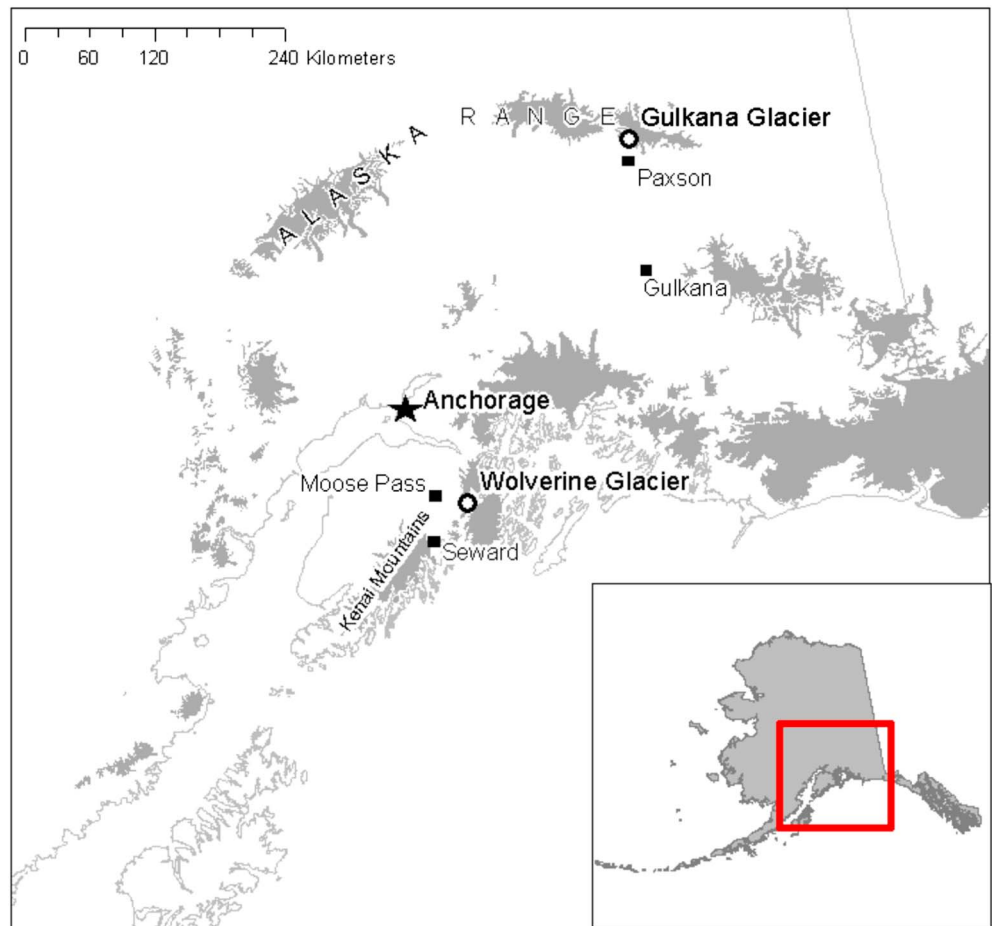
Wolverine Glacier and its surrounding basin are in the coastal Kenai Mountains of south-central Alaska in a maritime climate regime with high precipitation rates. Glacier mass turnover rates are high. In 2011, the glacier encompassed 66% of its 24.5 km² basin [*O'Neel et al.*, 2014]. Characteristic of maritime glaciers, it is highly sensitive to changes in temperature and precipitation [*O'Neel et al.*, 2014].

Gulkana Glacier and its surrounding basin are located in the eastern Alaska Range in a continental climate regime. Glacier mass turnover rates are much lower than at Wolverine Glacier, as it is colder and has lighter, irregular precipitation. This basin contains three other smaller glaciers with multiple branches and a terminus that is heavily covered with rock debris [*Van Beusekom et al.*, 2010; *Josberger et al.*, 2007]. In 2011, the main glacier (Gulkana) encompassed 53% of its 31.5 km² basin [*O'Neel et al.*, 2014]. Gulkana Glacier is less steep than Wolverine, especially at the terminus. Later figures and cited references give specific measurements on Gulkana Glacier, as well as Wolverine.

3.1. Existing Hydrological Simulation Code

PRMS is a modular, deterministic, distributed-parameter, physical-process simulation code that is used to simulate land-surface hydrologic processes, including evapotranspiration, runoff, infiltration, shallow subsurface, groundwater, snowpack, and soil moisture, based on inputs of distributed daily maximum and minimum temperature and precipitation. The model calculates solar radiation (SR) and potential evapotranspiration (PET). PRMS simulates hydrologic water budgets at the basin scale with temporal scales ranging from days to centuries. Figure 2 shows PRMS with the glacier module enhancement (PRMSGlacier).

The spatially distributed parameter capabilities of PRMS are provided by partitioning the basin into Hydrologic Response Units (HRUs). Each HRU is characterized by a suite of parameters describing its topography, soils, vegetation type and density, and imperviousness. Each HRU is assumed to be homogenous with respect to its hydrologic response and should therefore be delineated to accommodate the dominant process in that location. PRMS HRUs are conceptualized as a series of reservoirs that include the soil zone, shallow subsurface, and groundwater reservoirs, whose outputs are combined to supply streamflow. PRMSGlacier adds to this an HRU-based glacier storage. For each HRU, a water balance is computed each day and an energy balance is



Glacier boundaries from the Alaska Department of Natural Resources (http://dnr.alaska.gov/mdfiles/glacier_2mil.html, accessed October 20, 2015).

Figure 1. Locations of Wolverine and Gulkana Glacier basins and selected cities.

computed twice each day. All fluxes from an HRU are routed to a single segment in a stream network. Once in the network, water is routed to the basin outlet.

4. Conceptual Overview of Glacier Simulation Enhancements

In order to facilitate the simulation of these new glacier processes, an additional type of HRU (*glacier-capable*) has been defined for PRMSGlacier and used to create spatial subdivisions of any glacier in the basin based on elevation. The glacier module is driven with inputs of daily precipitation and maximum and minimum air temperature, and PRMS-computed daily solar radiation. Although PRMS and the majority of these glacier simulation enhancements are being calculated on a daily basis, there are several glacier “evolution” characterizations, described below, that are performed on an annual time step.

In any given year, the model keeps track of glacierized HRUs and HRUs that represent the current terminus of the glacier. Although change in per-HRU glacier volume is simulated on a daily basis, the glacier area (the aggregation of glacierized HRUs) is assessed on an annual basis. The sequence by which glacier growth and retreat occurs through HRUs is inferred based on relative HRU elevation. The reduction in glacier extent for a given year is first taken from the terminus HRU, and then the nearest upslope glacierized HRUs (the opposite sequence applies for increases in glacier size). Areal changes higher on the glacier are not simulated. The glacier area may extend to the next downslope glacier-capable HRU, but not into nonglacier-capable (land surface) HRUs. All HRUs upslope from the HRU that contains the glacier terminus are fully glacierized. Because the terminus HRU is only partially glacierized, the nonglacierized portion of the HRU behaves like a standard land-surface HRU. If the downstream-most glacier-capable HRU area becomes 100% covered, no further increase

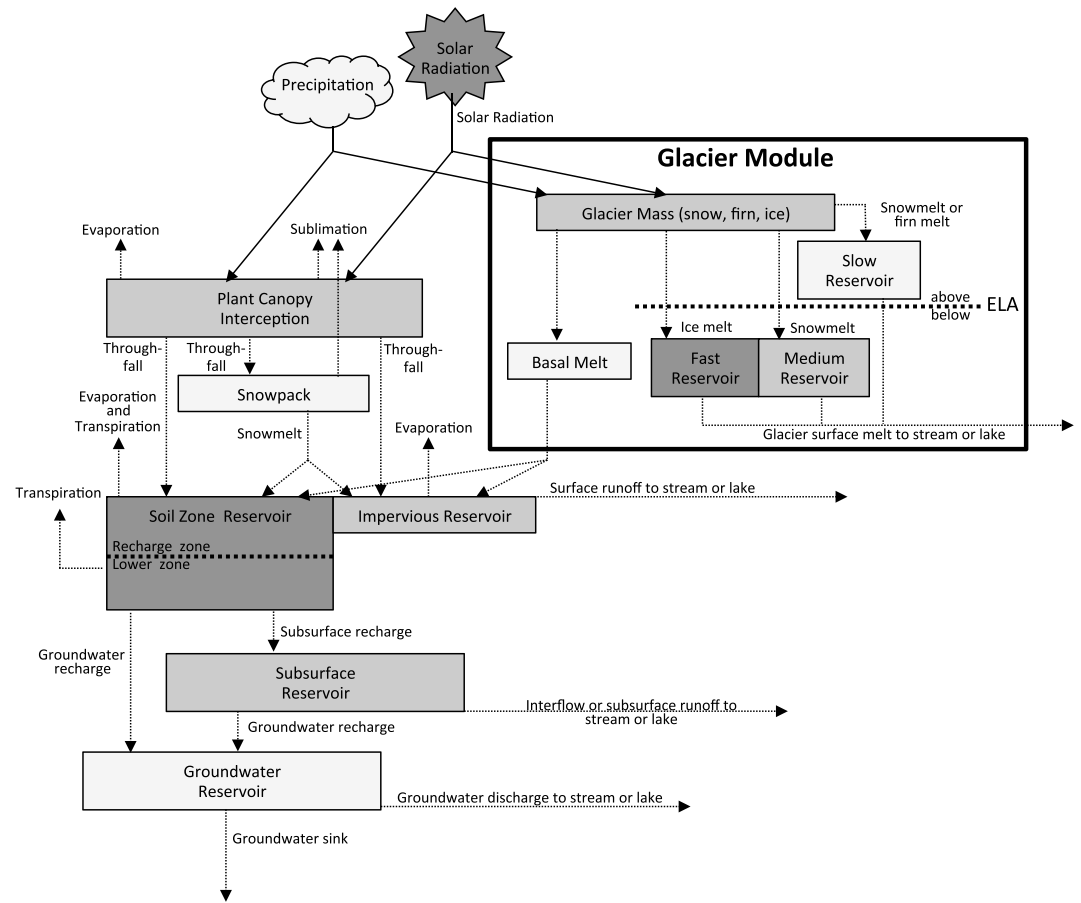


Figure 2. Overview of the PRMSglacier conceptualization of basin components and fluxes (adapted from Markstrom et al. [2008]).

(that is, positive change) in volume will be simulated. Snow incident to a terminus HRU is divided into glacierized and nonglacierized snowpack based on the fraction of HRU area covered by glacier in that year.

Standard HRUs (which are not allowed to be glacierized) build a snowpack on the soil or rock surface of the land. Melting snowpack infiltrates directly into the HRU soil zone or runs off into the drainage network as a result of soil saturation or infiltration excess. Standard HRUs do not simulate the state of glaciers. If designated as an HRU as glacier-capable in the parameter file, the melt from the HRU will contribute to an additional set of three reservoirs representing slow, medium, and fast rates of flow through the glacier based on the method of Baker et al. [1982]. The current manuscript uses the slow, medium, and fast labels for these reservoirs, but they are often called the firn, snow, and ice reservoirs, as they conceptually represent the hydraulic properties of water flowing through each medium. This is a conceptual model of flow embedded in a glacier (englacial flow); although, no explicit simulation of englacial flow routing exists in the module. Instead, daily outflow from each of these reservoirs for a glacierized HRU is routed to the stream segment associated with the terminus HRU, bypassing any stream segments directly associated with the source HRU (as would be used in standard PRMS).

There is a constant rate of basal melt that is subtracted from the glacier mass and pushed into the HRU land surface. The standard PRMS processes infiltrate the basal melt into the HRU soil zone reservoir, store it in the HRU impervious land surface reservoir, or convert it to runoff (if the preceding reservoirs are full or the basal melt rate exceeds the infiltration rate of the soil zone). PRMSglacier allows flexibility in the definition of the network of stream segments, which enables direct tracking of flows that move or originate beneath the glacier. This is a simplified form of subglacial routing that does not capture any dynamic interactions between subglacial streams and the overlying glacier, such as refreezing, hydraulic barriers, or englacial routing. Branches of the network may start on the land surface, pass beneath the glacier, and emerge from under

the glacier, with any combination of tributaries. Segments may also initiate entirely beneath the glacier. Examples are shown in the section 7.

The overall glacier content of an HRU is tracked as snow and ice by the module. Firn is not specifically modeled; any snowpack on an HRU when the date transitions from 30 September to 1 October (the start of the hydrologic water year (WY)) is treated by PRMSGlacier as ice with regard to the energy balance of that water volume. In terms of which types of melt are routed to the different glacier reservoirs, any melting from glacierized HRUs above the equilibrium line altitude (ELA) goes to the slow reservoir, snow melting from an HRU below the ELA goes to the medium reservoir, and ice melt below the ELA goes to the fast reservoir, as in *Hock and Noetzli* [1997]. The ELA, and the designation of which HRU it falls within, is reset annually by finding the HRU whose annual melt is closest to its total snowfall. Any melt from a glacierized HRU that contains the ELA for a given year is routed to the medium reservoir.

5. Module Detail

5.1. Glacier-Influenced Runoff Computation

5.1.1. Glacier Surface Melt

PRMSGlacier requires input of glacier surface melt. This is provided by modification of the PRMS snow module by melting glacial ice and snow (that is, daily ablation or accumulation). Glacier surface melt is expressed as the change in the snowpack/glacier height on each glacierized HRU. The original snow module uses an energy balance model based on the equations of *Anderson* [1968]; after modification for glaciers, the governing equation for any time increment is

$$H_{\theta} = H_r + H_s + (H_e + H_l) + H_c + H_w, \quad (1)$$

where H_{θ} is the change in heat storage of the glacier; H_r is the shortwave and longwave radiation heat flux; H_s is the sensible heat flux; H_e and H_l are the latent heat flux from evaporation, condensation, or sublimation, and by freezing or melting, respectively; H_c is the conductive-energy flux in between the snow surface layer, snow layer, ice layer, and the ground in turn; and H_w is the heat flux by gain or loss of water. For each HRU, the snow module executes the following five steps daily:

1. compute the amount of incoming precipitation and energy changes due to precipitation (H_w) and ambient temperature (H_s) on the snowpack or exposed ice layer;
2. estimate the change in snow-covered area;
3. estimate the change in albedo for snow surface or ice surface;
4. apply the remainder of the energy budget (radiant (H_r), convective (H_l), and conductive (H_c) exchanges) to snowpack or exposed ice layer energy budget; and
5. estimate the energy changes due to evaporation from snowpack or exposed ice layer (H_e).

Note that snowmelt is produced as a result of what happens in steps (1) and (4). Internal accumulation with refreezing happens in these steps also. All water freezes in the snowpack or exposed ice layer until the heat storage becomes zero, after which point liquid water fills the free-water capacity, with the excess becoming runoff.

The PRMSGlacier snow module first melts the snowpack, which consists of a surface and subsurface snow layer. The snowpack sits over an ice layer. This ice layer does not absorb energy (assumes that portion of H_c is 0) and has zero free-water holding capacity (not participating in H_w). Because conduction has been shown to be most important within the snowpack [*Pellicciotti et al.*, 2009], it is assumed that there is no significant conduction between the ice layer and the ground or even between the snowpack and the ice layer. Once the snow is gone, the ice layer is treated as an infinitely deep snowpack with a shallow layer that absorbs energy that now has a small free-water holding capacity, a high density, and a low albedo, referred to here as the *active layer*. Note that this is in contrast to freshly deposited snow in PRMS, which starts out with low density and high albedo, and progresses toward higher density and lower albedo with time. The active layer is a simplification of specifically tracking firn and changing density of snow/firn after 1 year. The thickness of the active layer starts each WY at a consistent value for all glacierized HRUs. This value is constrained to the range of 0–15 m and is generally set based on calibration [*Cuffey and Paterson*, 2010]. PRMSGlacier calculates conduction within both the snowpack and any exposed active ice layer. Rather than assuming temperature of top of the exposed active layer is 0°C, which has been shown to overestimate early season melt [*Pellicciotti et al.*, 2009], it is set to the average air temperature in the HRU for the last year. Once the active

layer has melted, the ice below is zero degrees and unable to hold free-water (referred to here as the *isothermal layer*). As mentioned in the conceptual overview of the module, snow that has not melted away during the summer is defined as ice at the beginning of each WY. The volume and energy of rain are integrated into that of the snowpack as well as the glacier ice.

Although PRMS can use measurements of incoming shortwave SR (for calculating H_r), these data are not commonly available. In their absence, PRMS calculates these from temperature and precipitation inputs with parameters (Table 1). The reflected shortwave SR is now calculated for ice, in addition to snow. The longwave radiation (for calculating H_l) is modeled by using the standard PRMS implementation of the Stefan-Boltzmann relation; incoming radiation is adjusted from perfect blackbody reflectivity with a calibrated emissivity factor, and outgoing assumes perfect blackbody reflectivity [Oke, 1987]. All calculations of SR flux take into account cloud-cover as estimated from incoming and potential SR and daily temperature range, also using the standard PRMS method [Thompson, 1976].

The newly added calculation of per-HRU glacier surface albedo, α , calculated from the empirical equation of Oerlemans [1992]:

$$\alpha = \alpha_s(t) - [\alpha_s(t) - \alpha_i] e^{-5d}, \text{ with ice albedo } \alpha_i = \bar{\alpha}_i + (\beta/\pi) \arctan[(E + 300)/200], \quad (2)$$

where $\alpha_s(t)$ is the time-variant snow albedo, d is the snowpack water equivalent (SWE) in meters, $\bar{\alpha}_i$ and β are calibrated constants, and E is the elevation (in meters) of the HRU above the ELA. Ice albedo is modeled as decreasing with decreasing elevation due to increasing probability of debris and dust deposits on the surface as the ice moves toward the terminus [Oerlemans et al., 2009]. The variable, E , will change annually as a function of changes in ELA (which is estimated based off the previous year's simulated MB). Surface albedo is constrained to the range of $0.08 \leq \alpha \leq 0.92$ if equation (2) produces a value outside this range [Brock et al., 2000]. Because of daily changes in HRU SWE (and annual changes in E), α will vary on a daily basis (if there is any snowpack present).

The daily changes in HRU glacier/snowpack height, HRU area, and snow density (or change to ice density) are used to calculate daily volume of melt to one of the glacier reservoirs (slow, medium, or fast). At daily time intervals, the discharge, Q , from a given reservoir at time t_2 (with inputs from t_1 the previous day) is

$$Q(t_2) = Q(t_1) e^{-24/k} + R(t_2) - R(t_1) e^{-24/k}; \quad (3)$$

where R is the rate of the water inflow (runoff) from the glacier into the reservoir and k is coefficient describing the lagging of flow out of the slow, medium, or fast reservoirs (k_f , k_m , or k_s , respectively). These lag coefficients are allowed to vary monthly to simulate changes in efficiency in the englacial routing throughout the melt season [Fountain and Walder, 1998; Hannah and Gurnell, 2001].

5.1.2. Glacier Basal Melt and Flow Under the Glacier

Basal melt is set at a rate of 12 mm yr^{-1} for all HRUs, 6 mm yr^{-1} of which is from geothermal heating, and 6 mm yr^{-1} is from friction between the glacier base and the land surface [Cuffey and Paterson, 2010]. This flux is routed to the HRU land surface (see Figure 2). The standard PRMS processes determine whether this volume infiltrates into the soil zone, is captured as impervious surface storage, or runs off to the nearest stream segment.

The PRMS runoff module will determine if the soil zone for a nonglacierized HRU is frozen using a simple temperature-based calculation of the Continuous Frozen Ground Index [Mastin, 2009; Molnau and Bissell, 1983]. The soil zone for glacierized HRUs does not freeze (simulating the glacier insulating it from the air temperature) with the exception of soil beneath the HRU where the glacier terminus resides, which is not fully insulated from colder air temperatures [Mooers, 1990].

5.2. Evolution of Glacier Landscape

5.2.1. Glacial Extent

PRMSGlacier simulates gains or losses in volume of the glacier mass on a daily basis. Glacier advance or retreat is simulated by changing the area of the glacier on the basis of this volume change. The module recalculates the glacier area at the end of each WY. The 1 year lag is not representative of realistic typical glacier area change but allows the module to simulate responses to extremely rapid changes in climate scenarios input [Raper and Braithwaite, 2009] and to be calibrated to area measurements that are taken at random intervals. A

Table 1. Parameters Calibrated in Each Step of the Calibration Process and Details of Each Step (Snow Parameters Light Gray, Glacier Parameters Dark Gray)

Step	Calibration Data Set	Objective Function (OF) Absolute Difference (AD) or Normalized Root-Mean-Square Error (NRMSE)	PRMS Parameters Used to Calibrate Model State	Parameter Range		Parameter Description (Most Units are SI)
				Min	Max	
1	Glacier mass balance	2 NRMSE OFs: Annual maximum and minimum	albedo_coef (β)	0.1	0.25	Coefficient in ice albedo calculation
			albedo_ice ($\bar{\alpha}_i$)	0.25	0.45	Ice albedo 300 m below ELA (fraction)
			emis_noppt	0.76	1.0	Emissivity of air on days without precipitation (fraction)
			glacr_layer	0.00	15	Thickness of active layer of glacier (m)
2	Daily flowtiming (all flows)	3 NRMSE OFs: daily, monthly mean, and annual mean	glacr_snow_adj	0.5	+1.5 ^a	Precip adjust factor correcting for gage undercatch, elevation lapse for snow days
			adjmix_rain	0.6	1.4	Factor to adjust rain proportion in mixed rain/snow event (fraction)
			cecn_coef	2	10	Convection condensation energy coefficient (calories/°C above 0)
			freeh2o_cap	0.01	0.2	Free-water holding capacity of snowpack (fraction)
			glacr_freeh2o_cap	0	0.01	Free-water holding capacity of active layer of glacier (fraction)
			potet_sublim	0.1	0.75	Proportion of PET that is sublimated from snow surface (fraction)
			rain_adj	0.5	+1.5 ^a	Precip adjust factor correcting for gage undercatch, elevation lapse for rain days (fraction)
			slowcoef_sq	0.001	0.1	Nonlinear coefficient in equation to route gravity-reservoir storage downslope
			soil_moist_max	0.13	0.25	Maximum available water holding capacity of soil profile (m)
			soil_rechr_max	0.025	0.13	Maximum available water holding capacity for soil recharge zone (m)
			stor_firn (k_s)	150	1000	Monthly storage coefficient for slow englacial flow (h)
			stor_ice (k_f)	5	29	Monthly storage coefficient for fast englacial flow (h)
			stor_snow (k_m)	30	149	Monthly storage coefficient for medium englacial flow (h)
			tmax_adj	-1.11	2.78	Maximum temperature adjustment factor indexed by HRU (°C)
			tmax_allrain	1.11	7.22	If HRU tmax exceeds this monthly value, precipitation assumed rain (°C)
			tmax_allsnow	-1.11	4.44	If HRU tmax is below this value, precipitation assumed snow (°C)
tmax_lapse	5.0	7.0	Decrease in maximum temperature (°C) with 1000 m			
tmin_adj	-2.78	1.39	Minimum temperature adjustment factor indexed by HRU (°C)			
tmin_lapse	5.0	7.0	Decrease in minimum temperature (°C) with 1000 m			
3	Daily flowtiming (high flows)	2 NRMSE OFs: Daily and monthly mean	fastcoef_lin	0.001	0.8	Coefficient to route preferential-flow storage downslope (fraction)
			pref_flow_den	0	0.1	Fraction of the soil zone in which preferential flow occurs
			sat_threshold	0.025	0.38	Water holding capacity of the gravity and preferential flow reservoirs (m)
			smidx_coef	0.001	0.06	Coefficient in nonlinear surface runoff contributing area algorithm (fraction)
4	Daily flowtiming (low flows)	2 NRMSE OFs: Daily and monthly mean	gwflow_coef	0.001	0.1	Fraction of groundwater daily discharge from groundwater storage
			ssr2gw_rate	0.05	0.8	Coefficient for routing water in gravity reservoir to groundwater reservoir (fraction)
5	SR	AD OF: Mean monthly	ccov_intcp	0	5	Monthly intercept in daily temperature range relationship for cloud cover
			ccov_slope	-0.9	-0.02	Monthly slope in daily temperature range relationship for cloud cover (°C)
			crad_coef	0.3	0.7	

Table 1. (continued)

Step	Calibration Data Set	Objective Function (OF) Absolute Difference (AD) or Normalized Root-Mean-Square Error (NRMSE)	PRMS Parameters Used to Calibrate Model State	Parameter Range		Parameter Description (Most Units are SI)
				Min	Max	
6	PET	AD OF: Mean Annual	jh_coef	0.005	0.09	Coefficient in <i>Thompson</i> [1976] relationship of cloud cover to SR Monthly air temp coefficient in Jensen-Haise PET computations ($^{\circ}\text{F}$ as traditional)
7	Glacier area	1 NRMSE OF: Annual mean	glacva_coef (\hat{c}) glacva_exp (γ)	0.1 1.31	1.5 1.44	Glacier volume-area power law coefficient ($\text{m}^{(3-2\gamma)}$) Glacier volume-area power law exponent

^aNot allowed to get any larger than initial maximum + 0.7.

power law relation of $V = cA^{\gamma}$, between a glacier's volume of ice V and area A , has been developed by previous researchers [e.g., *Bahr et al.*, 1997; *Chen and Ohmura*, 1990].

While theoretical considerations as well as measurements find that value of ~ 1.375 for the coefficient, γ , is suitable for many glaciers, the c coefficient lacks the same support for estimating its value and can lead to a poorly constrained value that varies greatly with region, glacier geometry, and climate [*Arendt et al.*, 2006; *Bahr et al.*, 2009; *Lüthi*, 2009; *Van de Wal and Wild*, 2001]. Rather than relying on a constant value of c for a basin through time, it is set for each glacier as at the end of the WY as follows: (1) the glacier is divided (by the HRU delineation process) into elevation bands; (2) for each band, the MB (b) is calculated (cumulative) over the WY; (3) two gradients between each consecutive pair of elevation bands are calculated. The first is the MB gradient, which is the change in MB with change in elevation from one band to the next, or db/dz . The second is the slope of the land surface beneath the glacier, that is the change of basal elevation (u_b) with centerline distance (x), or du_b/dx ; (4) the glacier-wide averages of these two gradients are then inserted into equation (4).

$$V = cA^{\gamma}; \text{ with } c = \hat{c} < db/dz >^{1/5} \tan[< du_b/dx >]^{-2/5}, \quad (4)$$

after *Lüthi's* [2009] theoretical suggestion as a way of making c more locally sensitive than relying on the single, constant value.

5.2.2. Basal Topography

An estimate of glacier basal elevation of each HRU is needed to compute the mean bed slopes (du_b/dx) in equation (4), as well as provide estimates of HRU land elevation, slope, and aspect for runoff computations in the event of ground exposure due to glacial retreat. Time t , surface elevation u_s , basal elevation u_b , glacier width w , specific mass flux q , rate of mass balance gain or loss b , and distance from the top of the glacier to a given location on the centerline x (referred to as *centerline distance*, with maximum centerline distance at the bottom of the terminus x_t) are inserted into the equation for the isothermal approximation with mass conservation [*Cuffey and Paterson*, 2010]:

$$\partial u_s / \partial t = (1/w) \partial (wq) / \partial x + b(x, t), \quad 0 \leq x \leq x_t. \quad (5)$$

The boundary conditions for equation (5) are that flux q is 0 at the top and the terminus of the glacier, and that the terminus surface elevation equals the basal elevation. After all variables in equation (5) are scaled to be of order of magnitude 1 ($O(1)$) such that $x^* = x/x_t$, $u_s^* = u_s/C$, and $u_b^* = u_b/C$, $w^* = w/w_0$, and $b^* = b/b_0$, q in equation (5) can be replaced with the shallow ice approximation of q^* [see *Cuffey and Paterson*, 2010]:

$$q^* = \text{sgn}(\partial u_s^* / \partial x^*) \left[\kappa (u_s^* - u_b^*) F_1(\sigma^*) + (u_s^* - u_b^*)^2 F_2(\sigma^*) \right], \quad (6)$$

where flux is a combination of glacier sliding with plastic flow around obstacles $F_1(\sigma) = \sigma^{(n+1)/2}$ and regelation (melting under pressure and refreezing when the pressure is reduced) $F_2(\sigma) = \sigma^n / (n+2)$. These are both functions of bed shear stress $\sigma = |\partial u_s / \partial x| (u_s - u_b)$ [*Kamb*, 1970], following *Mazo* [1995]. Functions $F_1(\sigma)$ and $F_2(\sigma)$ use a coefficient of creep $n = 3$ [*Hooke*, 2005], and equation (6) uses a scale-independent roughness κ [*Kamb*, 1970] $\kappa \sim 10^{-2} + 10^{-3}$ if variable is $O(1)$. The scaling constant C is defined:

$$C = (b_0 x_t^n + 1 / (2A(\rho g)^n))^{1/(2n+2)}, \quad (7)$$

using flow rate factor A ($A = 3.2 \times 10^{-18} \text{ Pa}^{-3} \text{ yr}^{-1}$ from *Cuffey and Paterson* [2010]), ice density ρ , and acceleration due to gravity g .

Define the MB at each point along the centerline as $\underline{b}^*(x^*)$, and the total accumulated mass to that point as $B(x^*)$, where

$$B(x^*) = \left(\int_0^{x^*} w^*(a) \underline{b}^*(a) da \right) / w(x^*), \quad (8)$$

If the glacier is in a steady state MB, then the change in elevation of the glacier surface over time, $\partial u_s / \partial t$, becomes 0. Assuming steady state in equation (5) and integrating over x , equation (5) is transformed to

$$0 = \kappa(u_s^* - u_b^*) F_1(\sigma^*) + (u_s^* - u_b^*)^2 F_2(\sigma^*) - B(x^*), \quad (9)$$

which can be solved for u_b^* and thus basal elevation u_b . Although equation (9) is ideally solved as an optimization problem if the glacier is not in steady state, this optimization problem is highly unstable in one dimension [Mazo, 1995; Salamatin and Mazo, 1985], and although expanding the problem to two dimensions is more stable, is computationally expensive [Clarke et al., 2013; Michel et al., 2014]. PRMSGlacier avoids these issues by solving the problem in one dimension (as in equation (9)) and estimating a steady state glacier MB. The steady state MB is estimated by using the MB gradient calculated from the first year of simulation as the shape of the steady state MB gradient and shifting the function $b(z)$ up or down in elevation z so that the glacier net MB is zero. This approach relies on the further assumption the surface elevation at any point in time is not substantially different from the steady state shallow ice surface. Then, equation (9), along with boundary condition $u_b^*(1) = u_s^*(1)$, is solved for basal elevation with a finite difference scheme.

While the inputs to equation (9) are initially derived for each glacierized HRU (the details of deriving glacier surface elevation u_s , length x_t , and width w are described in section 5.3), cubic splines are applied to describe the change in each of these sets of values over the glacier. Equation (9) is solved at 100 points, resplined, and then each HRU is assigned the value of the centerline basal elevation solution at the midpoint of the HRU. These HRU centerline basal elevations are used in conjunction with the assumption of a parabolic glacier cross section (as in Harbor [1992]; $w(x) \propto (u_s - u_b)^p$) to infer the HRU average elevation of the bare earth land surface beneath the glacier. The model assumes an exponent of $p = 1.5$ for the HRU at the highest elevation band of the glacier, increasing linearly to a value of $p = 2.1$ at the terminus (glacierized) HRU. This coefficient approximates the effects of increasing intensity of erosion down-glacier and the expected deeper, narrower channel morphology in this direction [Graf, 1970].

5.3. Overview of Analyses for Delineation and Parameterization of Geographical Features

The PRMSGlacier application requires the delineation of HRUs and stream segments for both the glacier-capable and nonglacier-capable parts of the study areas. While there is ultimately a large degree of flexibility in the configuration of these features, the spatial delineations presented here are conceptually consistent with how the glacier physics is conceptualized and implemented into software algorithms. Topographic analysis of digital elevation models (DEMs) was used to derive the upstream area above the downstream-most gage in each basin. A threshold applied against a flow-accumulation surface was used to define a preliminary network of drainage segments, as well as contributing areas associated with each segment. Contributing areas are split into “left-bank” and “right-bank” areas by using the segment to define preliminary HRUs that are consistent with the methodology typically used for land-surface type HRUs.

Because the glacier surface depicted in the DEM can vary from a concave shape, which is generally expected by standard topographic analyses of elevation, to a convex one, special steps were taken to delineate more appropriate HRUs on and near the glacier. In addition to defining elevation band-based HRUs within the current glacier extent, elevation bands were defined for an extension to each glacier that is intended to encompass the maximum possible extent to which a glacier might grow. To do this, the shape of the terminus of each preexisting glacier within the basin is isolated in a raster data set whose cell size matches that of the DEM. This shape is typically a crescent that is approximately one cell across, although this can vary slightly. This shape is then dragged downslope, following the DEM-derived flow direction, an arbitrary distance. The overall silhouette created by this process is used to define the extension. Although this shape might be likely to change as a function of changing land surface morphology, this potential source of error was deemed acceptable. The full set of glacier-capable HRUs, regardless of whether they are glacierized at the start of the period of simulation, are superpositioned onto the preliminary map of land-surface HRUs (that is, replacing portions of and not intersecting with the preliminary map) to finalize the HRUs. A subglacier

set of segments are defined as a centerline for each glacier and added to the topographically derived segment network, as well.

New model parameters specific to glacier-capable HRUs include a measure of HRU effective width and length, which is descriptive of the portion of the overall glacier within the HRU, and are used in calculations of the basal elevation. The effective width is set as 2 times the major axis of the largest ellipse to fit inside each glacier-capable HRU. Length of an HRU is computed as area divided by the effective width. This will underestimate the actual width and overestimate actual length. The underestimated width is desirable because it is only the width the 1-D physics operates on, ignoring the side drag of the glacier [Farinotti *et al.*, 2009; Li *et al.*, 2012]. A parameter describing the initial fraction of glaciation of an HRU is also derived based on the digitized glacier outline (DGO). The value of this parameter is 1.0 inside the glacier outline, somewhere between 0.0–1.0 at the terminus HRU and 0.0 inside the glacier extension.

5.4. PRMSGlacier Calibration

Analyses were run for parameters that could only be resolved on the basis of values reported in the literature to determine the sensitivity of the model outputs to them. A single-parameter Monte Carlo sensitivity analysis was conducted to identify parameters that influence streamflow (also SR and PET). Those results were then used to specify the inputs to Fourier Amplitude Sensitivity Testing (FAST) [see McRae *et al.*, 1982; Reusser *et al.*, 2011], which targeted sensitivity of glacier MB, in addition to streamflow timing. FAST is a variance-based global sensitivity analysis that considers parameter interaction. Many parameters influence both MB and streamflow; the parameters were divided by the dominant variable each influenced the most.

For each basin the parameters were then calibrated using the Luca software [Hay and Umemoto, 2006]. Luca uses a multiple-objective, stepwise, automated calibration strategy with the Shuffled Complex Evolution global search algorithm [Duan *et al.*, 1992, 1994]. This multiple-objective, stepwise calibration procedure assures that intermediate model fluxes as well as the water balance are simulated consistently with measured values [Hay *et al.*, 2006]. Each step is focused on a major hydrologic process; the sequence here was (1) MB, (2) streamflow timing, (3) high flows, (4) low flows, (5) SR, (6) PET, and (7) glacier area. Each parameter was separated into a calibration step on the basis of which process is most sensitive to it (see Table 1). Since changing parameters may affect processes beyond the one being focused on within a given step, the sequence of steps is re-run over five successive rounds to search for parameter changes that balance the various objective functions. Calibrations are made over the even-numbered WY in the range of 1968 to 2009. The odd-numbered years in this range are used for evaluation (1966 and 1967 are used for model initialization).

6. Data Sets

6.1. Input Data Sets

Glacier extent and height are needed to derive the elevation of the land surface beneath a given glacier. Ideally, the DEM and the DGO would depict the land glacier state reflecting the start of the simulation period in order to simplify calculation of the basal topography. This was not the case for the two sample basins. The simulation started in 1966, the DGOs for the two basins were from the 1970s, and the DEM (whose data would indicate glacier height) came from approximately 2006 [Le Bris and Paul, 2015]. Glacier area was smaller in the 1970s than in 1966, and glacier heights were generally lower in 2006 than in 1966 (moreover, the height in 2006 was bare-earth elevation for some areas that were glacierized in 1966). As a result of these temporal mismatches in the source data, expert interpretation of field sketches and estimated areas [from Meier *et al.*, 1971], and mean annual elevation change by altitude [from Le Bris and Paul, 2015], was used to manually estimate the extent and elevations of glaciers within the basins in 1965. The resulting maps were then used to parameterize HRUs in the PRMS applications.

Daily precipitation and maximum and minimum temperature are the only inputs required to drive the model; there needs to be at least one value of each of these for each day the model is run. The spatial distribution of the values is handled in the model with elevational lapse coefficients and HRU adjustment factors. In the applications in this manuscript, on-glacier climate records at both glaciers exist for WY 1965–2010; these data are used as the model input with some adjustments described here. Gaps in the on-glacier records have been filled by using regional records to create a continuous record for WY 1965–2010. In addition, precipitation factors were developed to distribute the precipitation observed at the gages to HRUs based on elevation.

This work was documented in *Van Beusekom et al.* [2010]. The factors are used as the model's initial values for snow and rain adjustment parameters (Table 1).

The long-term temperature record is from station-based observations for the period WY 1965–2010. These records only contain a daily mean temperature, but PRMS requires daily maximum and minimum temperatures. The needed values were inferred by applying an annual curve of adjustment to the daily mean values. This curve was constructed by using patterns in records from newer temperature observations that are available on both glaciers, located in the same places as the long-term stations. The multiple temperature records were recorded for each glacier over 2.5 years at a time interval of 15 min. There were three probes at Gulkana (all data assigned to USGS weather station 15478038) and two probes at Wolverine (all data assigned to USGS weather station 15236895) for the period of October 2012 to March 2015. For each glacier, the probe with the smallest diurnal range in temperature was used to calculate daily minimum and maximum temperatures by (1) calculating the median daily maximum and minimum offsets from the mean for each of 12 months to make a monthly adjustment curve and (2) applying this adjustment curve to long-term record of daily mean temperatures.

6.2. Calibration Data Sets

For step one of the calibration process (glacier mass balance), the target data set for the simulation to match was net (annual minimum) and winter (annual maximum) MB on the largest glacier of each basin (Wolverine or Gulkana Glacier). This was computed annually from biannual measurements to track changes in glacier height, averaged from readings at 3–5 sites on each glacier [see *Van Beusekom et al.*, 2010] over the period of record (POR) 1966–2009 (data at <http://dx.doi.org/10.5066/F7HD7SRF>). The net balances have been estimated to be accurate to approximately ± 0.2 m. Several authors have suggested that the distribution of this error is expected to skew toward the negative end of this range and likely be even more negative than the -0.2 m threshold [*McGrath et al.*, 2015; *Van Beusekom et al.*, 2010]. For spring 2013, the winter MB values were 7–36% greater than more accurate radar measurements at Wolverine and 6–20% greater than more accurate radar measurements at Gulkana [*McGrath et al.*, 2015]. Because of the likely error in these “measured” MB values, the calibration of annual glacier mass balance simulated by PRMS at Wolverine is targeted to match them within a range of -5% to $+30\%$. The simulated annual net difference between the minimum and maximum MB values is only required to match the observed to within -0.4 m to $+0.2$ m. The calibration at Gulkana is targeted to match the annual winter balance to within -5% to $+20\%$ and the annual net -0.4 m to $+0.2$ m of observed.

For steps two to four (daily flow timing), the target data set was daily streamflow from either Wolverine Creek (USGS gage 15236900 for Wolverine) or Phelan Creek (USGS gage 15478040 for Gulkana). Streamflow records from the USGS National Water Information System network were pulled by using the USGS Downsizer [*Ward-Garrison et al.*, 2009] and separated into high and low flows with the Indicators of Hydrologic Alteration software [*Richter et al.*, 1996]. The POR for Wolverine Creek is WYs 1967–1978, 1981, and 2001 to present. The POR for Phelan Creek is WYs 1967–1978 and 1990–2010. Both of these gages are rated by the USGS as “poor” quality, meaning more than 15% error, so the records are used as calibration targets with a $\pm 20\%$ error range.

For step five (SR), the target data set was mean monthly SR values taken from the National Solar Radiation database [*National Solar Radiation Database*, 1992]. The National Solar Radiation Database uses observed values when available, and modeled otherwise. Mean monthly daily incoming shortwave SR values are given at cities near the glaciers (whose elevations are roughly 1000 m lower than the glaciers) for the periods of 1961–1990 and 1991–2010. Studies in the Alps showed that incoming shortwave SR measured in the mountains was 70–100% of the SR measured 1000 m below due to opposite effects of elevational insolation increase and cloud cover increase [*Marty et al.*, 2002]. Mean shortwave SR incident to the basins was computed by using a percentage of the nearest city SR value, with the percentage based on expert opinion. For Wolverine Glacier basin, 100% of the SR values at the city of Seward were used (see location in Figure 1). For the period of 1961–1990 when Seward observations were not taken, adjusted observations from Anchorage were used instead (using a ratio of 1991–2010 values at Anchorage and Seward). Near Gulkana Glacier, at West Gulkana Glacier (less than 2 km away, with similar topographic aspect) there are on-glacier measurements of incoming shortwave SR from the month of June–July in 1986 [*Brazel et al.*, 1992]. The values of these data are 82–89% of the data from the city of Gulkana during the same time. On

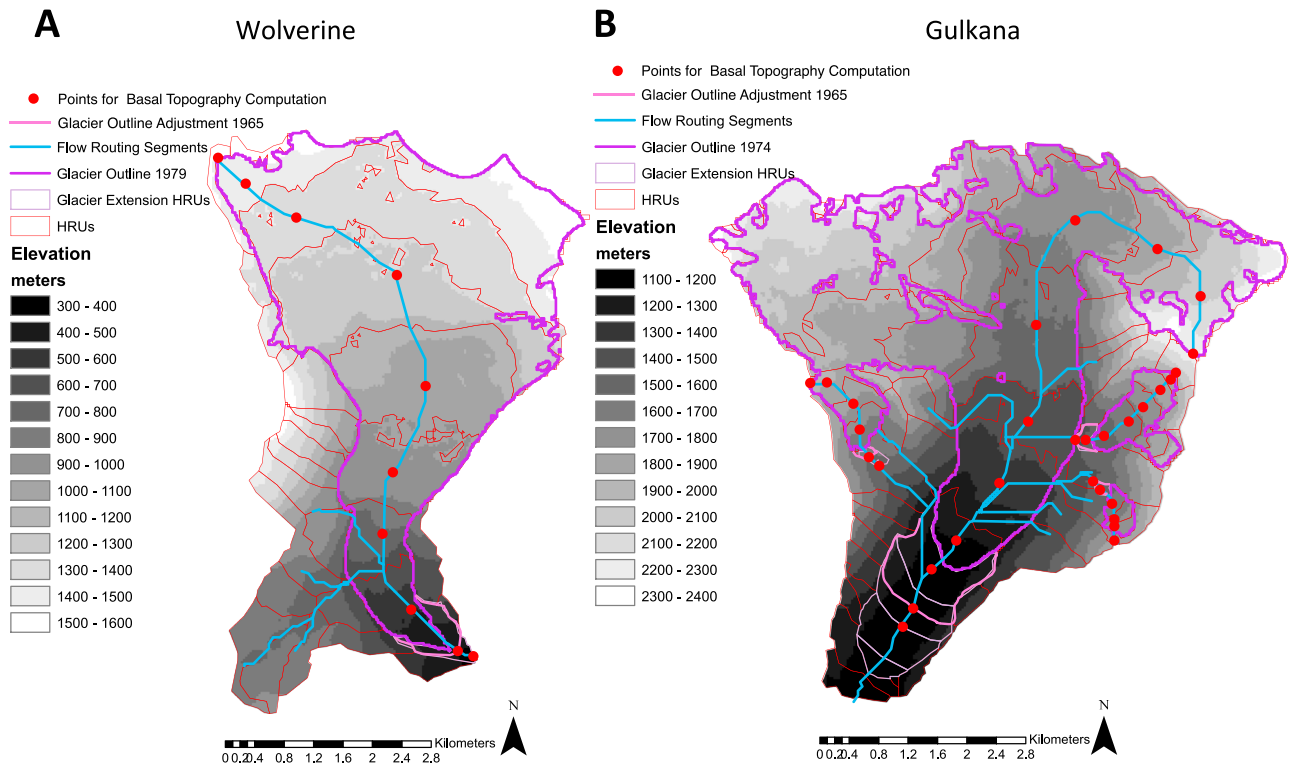


Figure 3. Flow routing segments, DGO, HRUs, and glacier extension HRUs with background of the DEM, for (a) Wolverine and (b) Gulkana Glaciers. Points used for basal topography (see Figure 4) are also shown.

the basis of this relationship, 85% of the global SR on measured from the city of Gulkana was used as the target for the SR calibration for Gulkana Glacier basin (see location on Figure 1).

For step six (PET), the target data set was the mean annual PET values taken from *Patric and Black* [1968], Moose Pass for Wolverine Glacier basin, and Paxon for Gulkana Glacier basin (see locations in Figure 1). For step seven (glacier area), the target data set was a set of annual glacier outlines that were interpolated for Wolverine Glacier from photogrammetric measurements or estimates made in WYs 1966, 1979, 1995, 1998, 2002, and 2011, and for Gulkana Glacier from measurements or estimates made in WYs 1967, 1974, 1993, 1999, and 2011 [see *Van Beusekom et al.*, 2010; *O'Neel et al.*, 2014].

7. Results

7.1. Model Setup: Routing Segments and HRUs

Although GIS preprocessing is not carried out by PRMSglacier, the results of this work are presented here as they are important to the model's proper functioning. The routing segments for the two sample basins are shown in blue on Figure 3. The respective delineations show how runoff from bare-ground HRU is routed into streams which eventually travel under the glacier, join the segments under the glacier centerline, emerge from under the glacier terminus HRU, and finally travel to the basin outlet. The centerline-type segments are similar to those defined in a study on the same glaciers by *Le Bris and Paul* [2013].

HRUs are also shown in Figure 3, with the glacier outline (purple lines) and the glacier extension (pink lines). Glacier-capable HRUs are within the combined extent of the glacier outline and extension. Those within the glacier outline begin the model simulation in a glacierized state. Because the glacier-capable HRUs are delineated by using elevation, there are some HRUs composed of multiple islands of high elevation that can be seen.

7.2. Basal Topography

Figure 4 shows the height of glacierized HRU surfaces, based on the constructed maps of glacier extent and height, at the start of the simulation, 1 October 1965, as gray dots connected with a (gray) spline. The

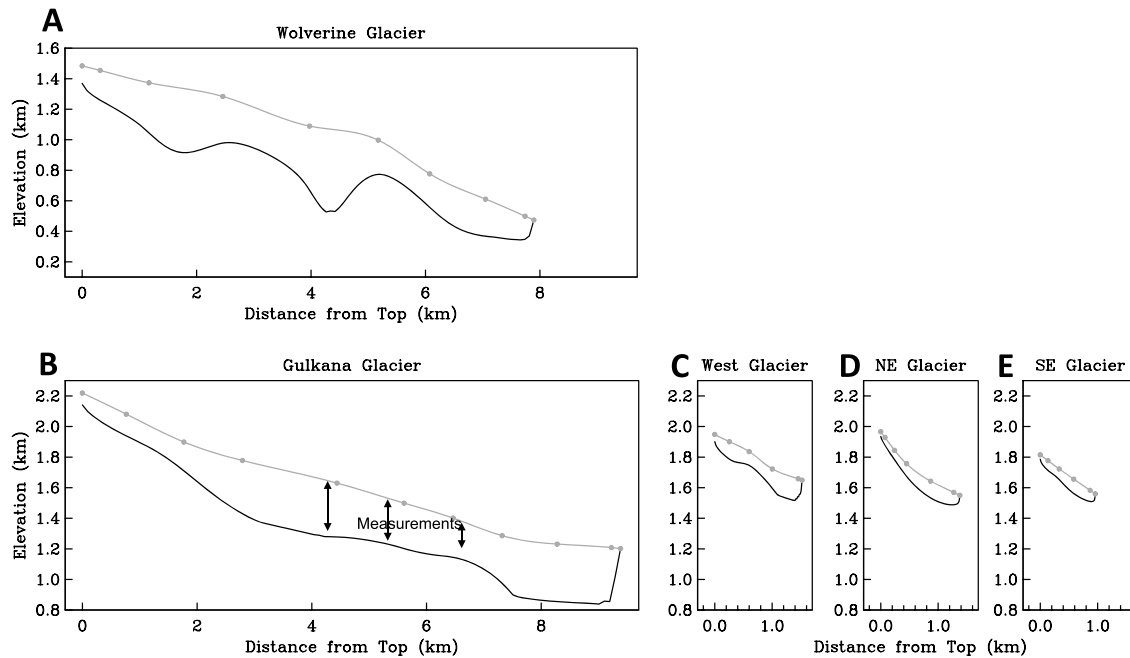


Figure 4. Glacier basal elevations from (a) Wolverine Glacier and (b–d) Gulkana basin glaciers (Figure 4b has three thickness measurements).

elevation of the glacier base/land surface was calculated on the basis of equations 5–8 and is shown as the black spline in Figure 4. Three field-based glacier thickness measurements available for the 1965 extent of Gulkana Glacier [Ostenso *et al.*, 1965] are shown on Figure 4, as the black arrows on the Gulkana Glacier plot.

7.3. Calibration and Evaluation

Measured and simulated values for the POR are shown in Figure 5. Simulated SR and PET values match observations almost exactly and are therefore not shown. Figures 5a and 5d show the measured and simulated streamflow at the gages as 3-monthly averages of daily values (October–December, January–March, April–June, and July–September) for Wolverine and Gulkana glacier basins, respectively. Measured streamflow values are shown with a shaded range calculated using the error described in the section 6.2.

Figures 5b and 5e track the MB for Wolverine and Gulkana Glacier, respectively, as change relative to the most recent minimum in the current or preceding WY, usually occurring during the preceding summer in the northern hemisphere. The simulation line breaks at each year as the datum from which change is calculated is reset. Measured values (gray points) are for the minimum and maximum MB value relative to previous minimum MB value. The error bars show the error range (described in section 6.2) for the measurements. In general, the simulation shows an increasing MB that peaks in late winter (the winter MB, usually in April–May) then progresses to a nadir (the net MB, usually in September–October).

Figures 5c and 5f show simulated glacier area as continuous function for Wolverine and Gulkana Glacier, respectively. It is changed only at the end of each WY to allow for adjustment lag (and so exhibits a step-function appearance). The filled circles are the actual measurements, and the open circles are annual values interpolated (or extrapolated) from those measurements.

The Nash-Sutcliffe efficiency (NSE) is a metric of model performance in predicting streamflow [Nash and Sutcliffe, 1970]. The daily NSE for each period is calculated as follows:

$$NSE = 1 - \frac{\sum (Q_m(t) - Q_s(t))^2}{\sum (Q_m(t) - \langle Q_m \rangle)^2}, \tag{9}$$

where $Q_m(t)$ is the measured daily streamflow, $Q_s(t)$ is the simulated daily streamflow, and $\langle Q_m \rangle$ is the mean of the measured daily streamflow over the period.

Two NSEs are calculated for each glacier, with and without error ranges of the measured values. Prior to calculation of the NSE using error ranges, $Q_s(t)$ is checked to see whether it falls within the $\pm 20\%$ error range of

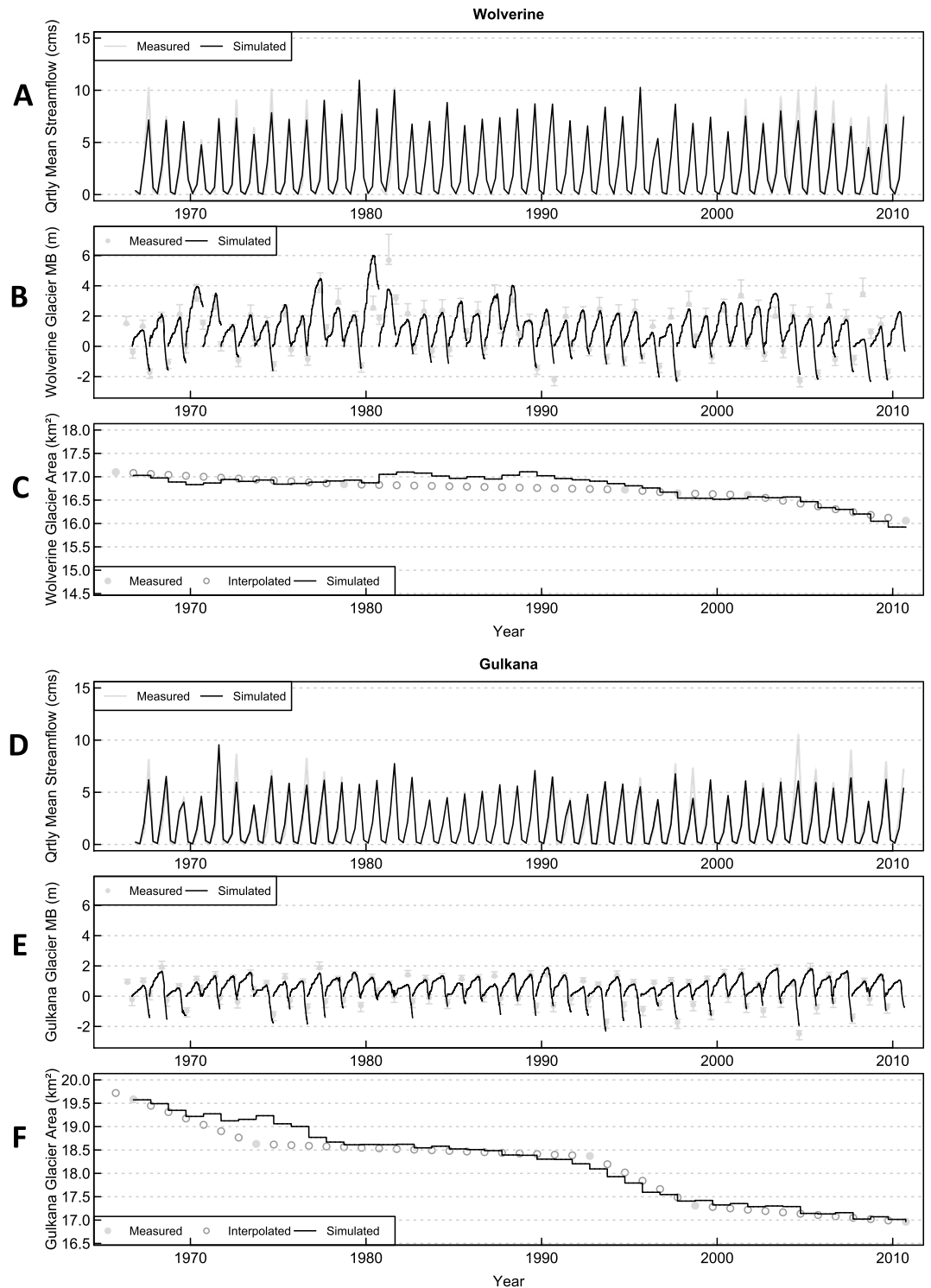


Figure 5. Results for the POR for (a–c) Wolverine Glacier basin and (d–f) Gulkana Glacier basin. Figures 5a and 5d show quarterly averages of daily streamflow.

$Q_m(t)$. If $Q_s(t)$ is inside the error range, then the measured streamflow for that day ($Q_m(t)$) is set to $Q_s(t)$ and the difference for that time step is 0. If $Q_s(t)$ is beyond the error range, $Q_m(t)$ is reset to the top or bottom of its error range in the same direction as $Q_s(t)$. Once this time series of adjusted-measured values is built, the NSE is calculated.

Table 2. Metrics of Model Performance for Calibration and Evaluation Periods for This Study and Others

Model Authors (Model Name)	Glacier Basin	Time Range for Metrics ^a	Variable	Metric	Calibration		Evaluation	
					No Error	With Error	No Error	With Error
This study (PRMSGlacier)	Wolverine, Alaska, USA	42 years	Streamflow	Daily NSE ^b	0.76	0.87	0.74	0.86
			Winter MB	Absolute bias fraction ^c	0.28	0.13	0.17	0.06
			Summer MB	Absolute bias fraction ^c	0.24	0.07	0.15	0.02
	Gulkana, Alaska, USA	42 years	Net MB	Average year value ^d	−0.50 m Sim., −0.26 m M.nE, −0.41 m M.wE			
			Streamflow	Daily NSE ^b	0.77	0.88	0.73	0.84
			Winter MB	Absolute bias fraction ^c	0.15	0.08	0.14	0.07
Immerzeel <i>et al.</i> , [2012] Huss <i>et al.</i> , [2010] (GERM)	Langtang, Nepal	7 years	Streamflow	Daily NSE ^b	0.76			
			Net MB	Average year value ^d	−0.86 m Sim., −0.52 m M.nE, −0.71 m M.wE			
	Rhonegletscher, Switzerland	50 years	Streamflow	Monthly, annual NSE ^b	0.96 monthly, 0.58 annual			
			Net MB	Average year RMS ^e	±0.36 m over entire 2-D surface			
Li <i>et al.</i> , [2015] (HBV)	Nigardsbreen, Norway	22 years	Streamflow	Daily NSE ^b	0.90		0.90	
			Net MB	Average year value	0.31 m Sim., 0.12 m Meas.			
	Chamkhar Chhu, Bhutan	11 years	Streamflow	Daily NSE ^b	0.87		0.85	
			Beas, India	Streamflow	Daily NSE ^b	0.65		0.73
Mayr <i>et al.</i> , [2013] (HBV-ETH)	Vernagtferner, Austria	9 years	Streamflow	Daily NSE ^b	0.89		0.83	
			Winter MB	Absolute bias fraction ^c	0.08		0.29	
			Summer MB	Absolute bias fraction ^c	0.12		0.45	
			Net MB	Average year value	−0.65 m Sim., −0.85 m Meas.			
Naz <i>et al.</i> , [2014] (DHSVM)	Bow River, Alberta, Canada	27 years	Streamflow	Daily NSE ^b	0.78–0.81		0.77	
			Net MB	Average year value	−0.81 m Sim., −0.85 m Meas.			

^aThe time range the metrics are computed over, from first year of computation to last; some middle years may not have measurements for computation.
^bNSE = 1.0 is perfect efficiency, and decreasing values are decreasing efficiency.
^cAbsolute bias fraction = 0.0 is perfect, and increasing values are decreasing goodness.
^dM.nE is measured no error considered; M.wE is measured with error considered.
^eRoot-mean-square (RMS) error is calculated over all surface grid cells and takes area errors into account.

For the MB, the maximum (winter MB) and maximum minus the minimum (summer MB) of each year from the simulation are compared to the measured values with absolute value of the bias as the metric of model performance. The annual bias fraction is computed as

$$\text{bias} = |(B_m(y) - B_s(y)) / B_m|, \tag{10}$$

where $B_m(t)$ is the measured annual maximum or maximum minus the minimum MB and $B_s(t)$ is the simulated annual maximum or minimum MB. To account for the error range in $B_m(y)$ (as discussed in the section 6.2), the same process of building time series of adjusted-measured values is applied before calculation of the bias considering error ranges.

The total NSE and mean biases for the whole calibration period (even WYs) and the whole evaluation period (odd WYs) are reported in the first rows of Table 2. This table gives the metric values based on the raw data, with no error range considered (“no error”) and the metric values with the error range considered (“with error”). The model was calibrated with an error range in the target data, so the performance compared to the data without this adjustment is poorer. Figures 6a and 6c show the NSE and bias fractions by year, all with the error range considered. The filled circles are the calibration years, and the open circles are the evaluation years. The streamflow simulated and measured with error ranges considered are compared by day and season in Figures 6b and 6d.

For ease of comparison, measured and simulated daily streamflow was averaged by day of year in the years that the measured and simulated records overlapped. This is a total of 21 years for Wolverine and 31 years for Gulkana (see the years with measured data in Figures 5a and 5d and NSE values in Figures 6a and 6c). The comparisons are shown in Figure 7. Also shown is the simulated glacier ice melt. Glacier melt includes any melt from snow that fell before the current WY, which is treated as ice by PRMSGlacier. Again, the measured streamflow values are shown with a shaded range calculated using the error described in the section 6.2.

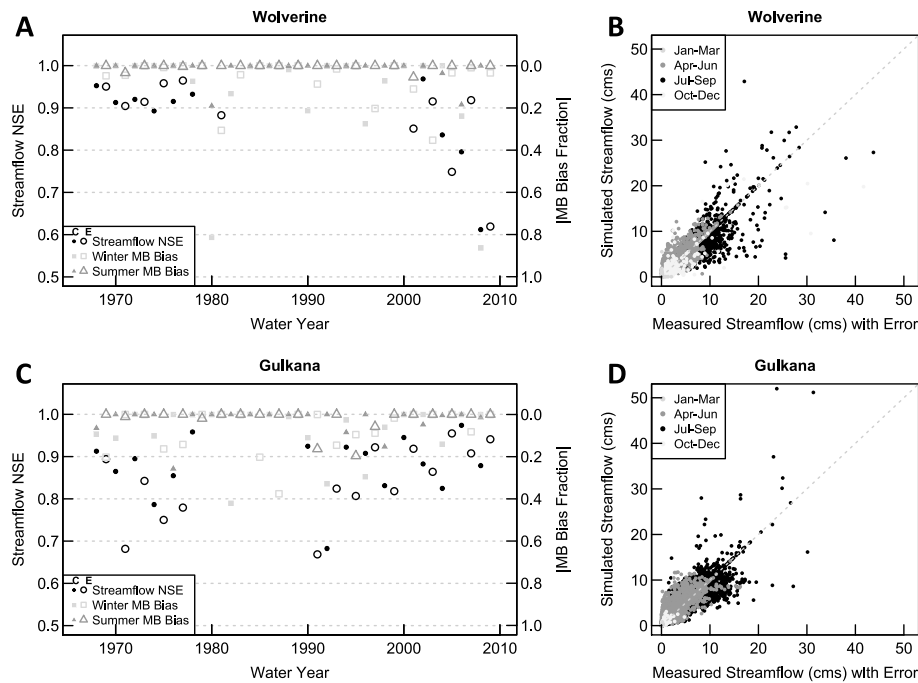


Figure 6. (a and c) The NSE of daily streamflow and absolute bias fraction of the MB by year for Wolverine and Gulkana, with the error considered in the measurements. (b and d) The daily simulated and measured streamflow plotted against each other.

8. Discussion

The test cases in this study show that the model does a very good job simulating glacierized basin hydrology for a long time period in two very different climatic regimes. Figure 6a shows some loss of model performance in the later years of Wolverine for streamflow and winter MB. At least some of this decline in performance can be attributed to problematic precipitation data used to drive the model for 2008, which showed almost no precipitation recorded despite the nearby city of Seward experiencing a “normal” year in terms of precipitation quantity. There is also an anomalous period in WY 1980–1981, which again appears to be a problem with the input precipitation data (it is vastly different than the observed pattern in Seward WY 1980–1981). The worst performance for Gulkana is in the middle of the POR (see Figure 6c). Neither of the models shows a large seasonal difference in performance for the majority of the days (see Figures 6b and 6d). But there are outliers and slight systematic underestimation of the daily flows in the 10–20 cm range in July–September. This underestimation is also seen in the mismatch of the streamflow peaks on Figures 5a and 5d. The average net MB is slightly more negative than the measured in both basins (see Table 2), which might be due to an underestimation of winter MB. The winter MB is largely controlled by the inputted precipitation amounts, which may need a larger adjustment than allowed in calibration (Table 1). Mismatches for higher values will necessarily look more egregious when plotted in absolute magnitude as in Figures 5, 6b, and 6d.

Overall, basin hydrology is better simulated if glacier behavior is constrained to keep the calibration process from spuriously compensating for errors in streamflow by (incorrectly) increasing glacier melt or accumulation [Mayr et al., 2013]. The calibration process used here optimized a set of performance metrics for a number of simulated states (measured streamflow and measured winter and net MB), rather than on any individual metric. This holistic approach likely reduced the goodness of fit for the individual states relative to the match that could be achieved if only one of the states was used, but the overall result is more accurate simulation of basin hydrology. In this model, underestimation of higher streamflow is likely due to the calibration trade-off between keeping the net MB from going too negative, given the winter MB, while matching the overall streamflow.

Table 2 shows the performance metrics of the applications compared to those achieved by other authors modeling these glaciers. None of the other models calibrate (or evaluate) with error ranges, so direct comparisons are not possible. The NSE values achieved in this study are comparable or better than those reported by

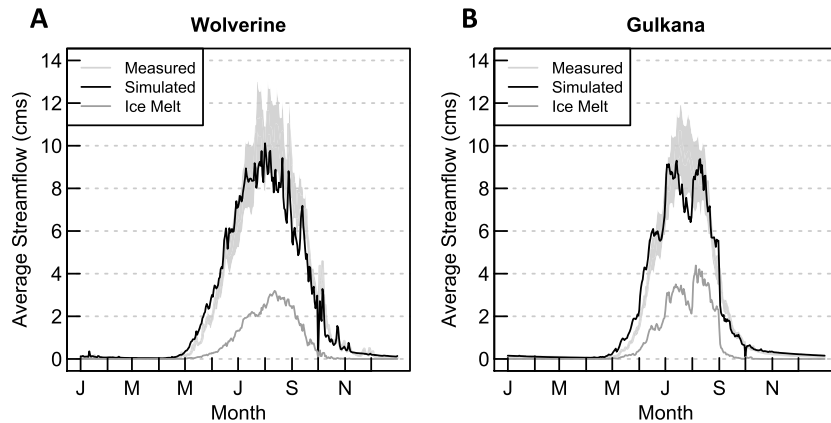


Figure 7. Measured daily streamflow, simulated daily streamflow, and simulated daily glacier ice melt, averaged over day of year for (a) Wolverine and (b) Gulkana basin.

the other authors. It is worth noting in this comparison that most of these other models were run for shorter time periods (Table 2) and therefore have not been exercised over as great a range of climatic and hydrologic conditions. These models also required more data input, expertise, and labor to apply. Apart from *Mayr et al.* [2013], these models do not or cannot calculate annual biases for winter and summer MB. The annual biases for these MB values are similar to the values achieved here. An alternate metric that is calculable from the results presented in these other studies is average net MB. This statistic can be misleading because although a model might simulate an average MB that closely matches the average measured MB, this can obscure that the model has both underestimated and overestimated MB during different points during the period of simulation. The MB biases for this study and the other comparable models are shown in Table 2, and again, the values here are similar.

PRMSglacier is useful because it allows the modeler to differentiate the glacier melt component of streamflow. It should be pointed out that the difference between the streamflow and glacier ice melt lines shown in Figure 7 does not characterize what the streamflow would look like if there was no glacier present in the basin, as the glacier adds basal melt to the soil, modifies the timing of the flow, and alters the local weather due to adiabatic winds [Cuffey and Paterson, 2010]. Figure 7 shows that a substantial amount of the streamflow in each basin comes from the melting of glacier ice, and this amount varies substantially in terms of timing and magnitude of flow across the two basins. This display shows how the importance of glacier ice melt as a component of streamflow decreases in the fall, likely being dominated by fall rains that are typical in the region. Furthermore, the relatively low input data requirements and computational cost of the model make it useable for a wide variety of research applications, such as projecting how glacierized hydrology will respond to various scenarios of climate change. Understanding how a basin responds to these changes is important for anticipating impacts on regional ecology [O'Neel et al., 2014].

8.1. Limitations

The design of PRMSglacier balances (1) explicit simulation of as many relevant processes as is possible with (2) expectations of the data that are available for most glaciated basins. There are a number of ways that the model methods for glacier simulation could be made more detailed or sophisticated. These relate to the energy balance, the assessment of glacier geometry evolution, the routing of melt within and out of the glacier, and the characterization of the elevation of the land surface beneath the glacier. The overall cost-benefit assessment of making these changes is not clear. Beyond increasing the input data requirements and increased effort required to apply the model, it is unclear whether the overall model performance would actually improve (or data to make this assessment are available).

Glacier MB is highly sensitive to albedo and emissivity. Although rigorous albedo algorithms exist (such as *Gardner and Sharp* [2010]), they tend to require substantial additional data and can only be estimated with large degrees of uncertainty. In addition, it has been shown that MB estimates derived by using a simple elevation-based albedo are similar to ones using field-based albedo measurements [Klok and Oerlemans, 2004], as was done here (see equation (2)).

Although estimating emissivity with vapor pressure gives substantially better simulations of MB [Juszak and Pellicciotti, 2013], these data are not readily available in most basins. Instead, this study calibrated emissivity coefficients for each basin to improve MB estimates over using a constant region-wide value, as indicated by Juszak and Pellicciotti [2013].

Because the model is built by using a three-layered representation of the glacier mass (snowpack, active layer ice, and isothermal ice) within each HRU, it can simulate the glacier subfreezing thermal profile of the active layer and helps to avoid overestimate melt as described by Pellicciotti *et al.* [2009]. Allowing for conduction of heat between layers and simulating the densification of snow to firn would be more physically realistic [Greuell and Oerlemans, 1986], but sensitivity tests indicated that this may not improve performance and would require generally difficult to define parameters.

Methods to explicitly simulate englacial melt routing exist [e.g., Flowers, 2008], but again, inputs for such models would not be well constrained in the majority of potential study areas. The conceptual model of englacial flow using parallel reservoirs has been shown to work remarkably well despite its simplicity [Jansson *et al.*, 2003]. Small improvements to the accuracy of the model might be made by dividing the glaciers into more HRUs, so that melt could be partitioned into the conceptual reservoirs more accurately. For subglacial routing, dynamic interactions between subglacial streams and the overlying ice have been studied on ice sheets but not extensively on glaciers [Jansson *et al.*, 2007]. Furthermore, subglacial flow contribution is small to the overall basin runoff timing [Stenborg, 1965]. Thus, investing further effort would likely not result improved overall model dynamics.

With the simple glacier area-evolution scheme, the calibrated model is able to match the actual measured area changes quite well through time (Figures 5c and 5f). Although glacier area might be better simulated with more accurate basal topography calculations, the advantage of the approach used here is that it does not require a long period of initialization (such as methods used in Clarke *et al.* [2015] and Naz *et al.* [2014]) or hard-to-acquire glacier thickness inputs (as in methods used in Farinotti *et al.* [2009], Huss *et al.* [2010], and Li *et al.* [2015]). Potential issues with this approach stem from the accuracy of representing the glacial mass-conservation with a one-dimensional solution (equation (5)) or from solving this (steady state) equation using estimates of MB and surface elevation that are not actually representative of the steady state.

These issues can cause inaccuracies such as those visible in the thick tongues of the glaciers in Figure 4. The area change lag time of a year needed for calibration is unrealistically short, however, using the more commonly used (but still arbitrary) decadal lag time was found to not substantially change streamflow, especially when area is changing monotonically.

Although the estimates of basal elevation for Gulkana results in glacier thicknesses that disagree slightly with depth soundings, these results are considered to be good, especially given that this elevation is very sensitive to the values used as the top of the glacier (which was manually estimated due to lack of observed values). This derived basal topography using a derived steady state MB is likely more accurate than one created using an assumed constant MB gradient for every glacier throughout large regions like Alaska, as has been done elsewhere [e.g., Farinotti *et al.*, 2009]. For use with PRMSGlacier, this basal topography approach is judged to be sufficiently accurate because it is summarized per HRU prior to usage in the simulations.

In terms of deriving glacier area from volume, setting the volume-area coefficient, c in equation (4), as a function of basal slope and MB gradient integrates the spatial and temporal variability of this quantity, which allows a better representation of individual glacier behavior (and addresses a shortcoming identified by Huss *et al.* [2010]). This was supported by the results of the sensitivity analysis and yields a model that relies more heavily on the better known γ parameter in place of the more empirical \hat{c} .

9. Conclusions

This study developed and tested an extension to an existing hydrologic simulation code, PRMS. The extension, PRMSGlacier, relies on physical principles as much as is feasible while maintaining model usability. Where possible, variables modeled with empirical coefficients were made more dependent on physical processes or characteristics; for example, albedo is calculated as a function of elevation and volume-area scaling is calculated as a function of basal slope and MB.

Despite the limitations of the glacier physics implementation and the available data, PRMSGlacier performed as well as or better than other more expensive models (in data and computation requirements) [e.g., Immerzeel *et al.*, 2012; Li *et al.*, 2015; Naz *et al.*, 2014; Mayr *et al.*, 2013]. The PRMSGlacier results also highlighted different kinds of performance than are traditionally shown in glacier-modeling papers (such as daily performance of streamflow in Figures 6 and 7 and winter and summer MB for each year in Figure 6), effectively demonstrating the robustness of this integration of glacier physics with general hydrologic modeling. The implementation of the glacier physics balances the need for operationally useful but scientifically rigorous integrated glacier-hydrology model. PRMSGlacier will allow much needed characterization and projection of hydrologic flows in large glacierized basins.

Acknowledgments

Output data are available on Science Base <https://dx.doi.org/10.5066/F75T3HMV> (sources for input data are cited in the manuscript). This work was supported by the Alaska and Northwest Climate Science Centers. We would like to thank our anonymous reviewers and our colleagues at the U.S. Geological Survey, including Timothy Brabets and Lauren Hay. Any use of trade, product, or firms names is for descriptive purposes only and does not imply endorsement by the U.S. government.

References

- Anderson, E. A. (1968), Development and testing of snow pack energy balance equations, *Water Resour. Res.*, *4*, 19–37, doi:10.1029/WR004i001p00019.
- Arendt, A., K. Echelmeyer, W. Harrison, C. Lingle, S. Zirnheld, V. Valentine, B. Ritchie, and M. Druckenmiller (2006), Updated estimates of glacier volume changes in the western Chugach Mountains, Alaska, and a comparison of regional extrapolation methods, *J. Geophys. Res.*, *111*, F03019, doi:10.1029/2005JF000436.
- Bahr, D. B., M. F. Meier, and S. D. Peckham (1997), The physical basis of glacier volume-area scaling, *J. Geophys. Res.*, *102*, 20,355–20,362, doi:10.1029/97JB01696.
- Bahr, D. B., M. Dyurgerov, and M. F. Meier (2009), Sea-level rise from glaciers and ice caps: A lower bound, *Geophys. Res. Lett.*, *36*, L03501, doi:10.1029/2008GL036309.
- Baker, D., H. Escher-Vetter, H. Moser, H. Oerter, and O. Reinwarth (1982), A glacier discharge model based on results from field studies of energy balance, water storage and flow, in *Hydrological Aspects of Alpine and High-Mountain Areas, Proc. Exeter Symp.*, edited by J. W. Glen, pp. 101–112, Wallingford, U. K.
- Bliss, A., R. Hock, and V. Radić (2014), Global response of glacier runoff to twenty-first century climate change, *J. Geophys. Res. Earth Surf.*, *119*, 717–730, doi:10.1002/2013JF002931.
- Brazel, A. J., F. Chambers, and L. Kalkstein (1992), Summer energy balance on West Gulkana Glacier, Alaska, and linkages to a temporal synoptic index, *Z. Geomorphol. Suppl. Band*, *86*, 15–34.
- Brock, B. W., I. C. Willis, and M. J. Sharp (2000), Measurement and parameterization of albedo variations at Haut Glacier d'Arolla, Switzerland, *J. Glaciol.*, *46*, 675–688.
- Chen, J., and A. Ohmura (1990), Estimation of Alpine glacier water resources and their change since the 1870s, *IAHS Publ.*, *193*, 127–135.
- Clarke, G. K. C., A. H. Jarosch, F. S. Anslow, V. Radić, and B. Menounos (2015), Projected deglaciation of western Canada in the twenty-first century, *Nat. Geosci.*, *8*, 372–377.
- Clarke, G. K., F. Anslow, A. Jarosch, V. Radić, B. Menounos, T. Bolch, and E. Berthier (2013), Ice volume and subglacial topography for western Canadian glaciers from mass balance fields, thinning rates, and a bed stress model, *J. Clim.*, *26*, 4282–4303.
- Cuffey, K. M., and W. S. B. Paterson (2010), *The Physics of Glaciers*, Academic Press, Oxford, U. K.
- Duan, Q., S. Sorooshian, and V. Gupta (1992), Effective and efficient global optimization for conceptual rainfall-runoff models, *Water Resour. Res.*, *28*, 1015–1031, doi:10.1029/91WR02985.
- Duan, Q., S. Sorooshian, and V. K. Gupta (1994), Optimal use of the SCE-UA global optimization method for calibrating watershed models, *J. Hydrol.*, *158*, 265–284.
- Farinotti, D., M. Huss, A. Bauder, M. Funk, and M. Truffer (2009), A method to estimate the ice volume and ice-thickness distribution of alpine glaciers, *J. Glaciol.*, *55*, 422–430.
- Farinotti, D., S. Usselman, M. Huss, A. Bauder, and M. Funk (2012), Runoff evolution in the Swiss Alps: Projections for selected high-alpine catchments based on ENSEMBLES scenarios, *Hydrol. Process.*, *26*, 1909–1924.
- Flowers, G. E. (2008), Subglacial modulation of the hydrograph from glacierized basins, *Hydrol. Process.*, *22*, 3903–3918.
- Fountain, A. G., and J. S. Walder (1998), Water flow through temperate glaciers, *Rev. Geophys.*, *36*, 299–328, doi:10.1029/97RG03579.
- Gardner, A. S., and M. J. Sharp (2010), A review of snow and ice albedo and the development of a new physically based broadband albedo parameterization, *J. Geophys. Res.*, *115*, F01009, doi:10.1029/2009JF001444.
- Graf, W. L. (1970), The geomorphology of the glacial valley cross section, *Arct. Alp. Res.*, *2*, 303–312.
- Greuell, W., and J. Oerlemans (1986), Sensitivity studies with a mass balance model including temperature profile calculations inside the glacier, *Z. Gletsch. kd. Glazialgeol.*, *22*, 101–124.
- Grossi, G., P. Caronna, and R. Ranzi (2013), Hydrologic vulnerability to climate change of the Mandrone glacier (Adamello-Presanella group, Italian Alps), *Adv. Water Resour.*, *55*, 190–203.
- Hannah, D. M., and A. M. Gurnell (2001), A conceptual, linear reservoir runoff model to investigate melt season changes in cirque glacier hydrology, *J. Hydrol.*, *246*, 123–141.
- Harbor, J. M. (1992), Numerical modeling of the development of U-shaped valleys by glacial erosion, *Geol. Soc. Am. Bull.*, *104*, 1364–1375.
- Hay, L. E., and M. Umemoto (2006), Multiple-objective stepwise calibration using Luca: U.S. Geological Survey Open-File Report 2006-1323 URL. [Available at ftp://brrcftp.cr.usgs.gov/pub/mows/pubs/hay_pubs/hay_pdf/luca_manual.pdf]
- Hay, L. E., G. H. Leavesley, M. P. Clark, S. L. Markstrom, R. J. Viger, and M. Umemoto (2006), Step wise, multiple objective calibration of a hydrologic model for a snowmelt dominated basin, *JAWRA J. Am. Water Resour. Assoc.*, *42*, 877–890.
- Hill, D. F., N. Bruhis, S. E. Calos, A. Arendt, and J. Beamer (2015), Spatial and temporal variability of freshwater discharge into the Gulf of Alaska, *J. Geophys. Res. Oceans*, *120*, 634–646, doi:10.1002/2014JC010395.
- Hock, R., and C. Noetzi (1997), Areal melt and discharge modelling of Storglaciären, Sweden, *Ann. Glaciol.*, *24*, 211–216.
- Hooke, R. L. (2005), *Principles of Glacier Mechanics*, Cambridge University Press, Cambridge, U. K.
- Huss, M. (2011), Present and future contribution of glacier storage change to runoff from macroscale drainage basins in Europe, *Water Resour. Res.*, *47*, W07511, doi:10.1029/2010WR010299.
- Huss, M., G. Jouviet, D. Farinotti, and A. Bauder (2010), Future high-mountain hydrology: A new parameterization of glacier retreat, *Hydrol. Earth Syst. Sci.*, *14*, 815–829.

- Immerzeel, W. W., L. P. H. van Beek, M. Konz, A. B. Shrestha, and M. F. P. Bierkens (2012), Hydrological response to climate change in a glacierized catchment in the Himalayas, *Clim. Change*, *110*, 721–736.
- Jansson, P., R. Hock, and T. Schneider (2003), The concept of glacier storage: A review, *J. Hydrol.*, *282*, 116–129.
- Jansson, P., J.-O. Naeslund, and L. Rodhe (2007), *Ice Sheet Hydrology—A Review*, Swedish Nuclear Fuel and Waste Management Co., Stockholm.
- Josberger, E. G., W. R. Bidlake, R. S. March, and B. W. Kennedy (2007), Glacier mass-balance fluctuations in the Pacific Northwest and Alaska, USA, *Ann. Glaciol.*, *46*, 291–296.
- Juszak, I., and F. Pellicciotti (2013), A comparison of parameterizations of incoming longwave radiation over melting glaciers: Model robustness and seasonal variability, *J. Geophys. Res. Atmos.*, *118*, 3066–3084, doi:10.1002/jgrd.50277.
- Kamb, B. (1970), Sliding motion of glaciers: Theory and observation, *Rev. Geophys.*, *8*, 673–728, doi:10.1029/RG008i004p00673.
- Klok, E. J., and J. Oerlemans (2004), Modelled climate sensitivity of the mass balance of Morteratschgletscher and its dependence on albedo parameterization, *Int. J. Climatol.*, *24*, 231–245.
- Le Bris, R., and F. Paul (2013), An automatic method to create flow lines for determination of glacier length: A pilot study with Alaskan glaciers, *Comput. Geosci.*, *52*, 234–245.
- Le Bris, R., and F. Paul (2015), Glacier-specific elevation changes in parts of western Alaska, *Ann. Glaciol.*, *56*, 70.
- Leavesley, G. H., R. W. Lichty, B. M. Troutman, and L. G. Saindon (1983), Precipitation-runoff modeling system—User's manual: U.S. Geological Survey Water-Resources Investigations Report 83–4238 URL. [Available at <http://pubs.usgs.gov/wri/1983/4238/report.pdf>.]
- Li, H., F. Ng, Z. Li, D. Qin, and G. Cheng (2012), An extended “perfect-plasticity” method for estimating ice thickness along the flow line of mountain glaciers, *J. Geophys. Res.*, *117*, F01020, doi:10.1029/2011JF002104.
- Li, H., S. Beldring, C.-Y. Xu, M. Huss, K. Melvold, and S. K. Jain (2015), Integrating a glacier retreat model into a hydrological model—Case studies of three glacierized catchments in Norway and Himalayan region, *J. Hydrol.*, *527*, 656–667.
- Lipscomb, W. H., J. G. Fyke, M. Vizcaino, W. J. Sacks, J. Wolfe, M. Verstein, A. Craig, E. Kluzek, and D. M. Lawrence (2013), Implementation and initial evaluation of the Glimmer Community Ice Sheet Model in the Community Earth System Model, *J. Clim.*, *26*, 7352–7371.
- Lüthi, M. P. (2009), Transient response of idealized glaciers to climate variations, *J. Glaciol.*, *55*, 918–930.
- Markstrom, S. L., R. G. Niswonger, R. S. Regan, D. E. Prudic, and P. M. Barlow (2008), GSFLOW, coupled ground-water and surface-water flow model based on the integration of the Precipitation-Runoff Modeling System (PRMS) and the Modular Ground-Water Flow Model (MODFLOW-2005) U.S. Geological Survey Techniques and Methods 6-D1:240 URL. [Available at <http://pubs.usgs.gov/tm/tm6d1/pdf/tm6d1.pdf>.]
- Markstrom, S. L., R. S. Regan, L. E. Hay, R. J. Viger, R. M. Webb, R. A. Payn, and J. H. LaFontaine (2015), PRMS-IV, the precipitation-runoff modeling system, version 4, US Geological Survey Techniques and Methods, 6-B7, 158 p., doi:10.3133/tm6B7.
- Marty, C., R. Philippon, C. Fröhlich, and A. Ohmura (2002), Altitude dependence of surface radiation fluxes and cloud forcing in the alps: Results from the alpine surface radiation budget network, *Theor. Appl. Climatol.*, *72*, 137–155.
- Mastin, M. C. (2009), Watershed models for decision support for inflows to Potholes Reservoir, Washington: U.S. Geological Survey Scientific Investigations Report 2009–5081, 54 p. URL. [Available at <http://pubs.usgs.gov/sir/2009/5081/pdf/sir20095081.pdf>.]
- Mayr, E., W. Hagg, C. Mayer, and L. Braun (2013), Calibrating a spatially distributed conceptual hydrological model using runoff, annual mass balance and winter mass balance, *J. Hydrol.*, *478*, 40–49.
- Mazo, A. B. (1995), Selection of a quasisolution of the problem of recovering the balance curve of an alpine glacier, *J. Math. Sci.*, *74*, 1246–1250.
- McGrath, D., L. Sass, S. O'Neel, A. Arendt, G. Wolken, A. Gusmeroli, C. Kienholz, and C. McNeil (2015), End-of-winter snow depth variability on glaciers in Alaska, *J. Geophys. Res. Earth Surf.*, *120*, 1530–1550, doi:10.1002/2015JF003539.
- McRae, G. J., J. W. Tilden, and J. H. Seinfeld (1982), Global sensitivity analysis—A computational implementation of the Fourier Amplitude Sensitivity Test (FAST), *Comput. Chem. Eng.*, *6*, 15–25.
- Meier, M. F., W. V. Tangborn, L. R. Mayo, and A. Post (1971), Combined ice and water balances of Gulkana and Wolverine Glaciers, Alaska, and South Cascade Glacier, Washington, 1965 and 1966 hydrologic years U.S. Geological Survey Professional Paper 715A:22 URL. [Available at <http://pubs.usgs.gov/pp/0715a/report.pdf>.]
- Michel, L., M. Picasso, D. Farinotti, M. Funk, and H. Blatter (2014), Estimating the ice thickness of shallow glaciers from surface topography and mass-balance data with a shape optimization algorithm, *Comput. Geosci.*, *66*, 182–199.
- Molnau, M., and V. C. Bissell (1983), A continuous frozen ground index for flood forecasting. In Proceedings 51st Annual Meeting Western Snow Conference, (Canadian Water Resources Assoc. Cambridge, Ont), pp. 109–119.
- Mooers, H. D. (1990), A glacial-process model: The role of spatial and temporal variations in glacier thermal regime, *Geol. Soc. Am. Bull.*, *102*, 243–251.
- Nash, J. E., and J. V. Sutcliffe (1970), River flow forecasting through conceptual models. Part I—A discussion of principles, *J. Hydrol.*, *10*, 282–290.
- Naz, B. S., C. D. Frans, G. K. C. Clarke, P. Burns, and D. P. Lettenmaier (2014), Modeling the effect of glacier recession on streamflow response using a coupled glacio-hydrological model, *Hydrol. Earth Syst. Sci.*, *18*, 787–802.
- Neal, E. G., E. Hood, and K. Smikrud (2010), Contribution of glacier runoff to freshwater discharge into the Gulf of Alaska, *Geophys. Res. Lett.*, *37*, L06404, doi:10.1029/2010GL042385.
- Nolin, A. W., J. Phillippe, A. Jefferson, and S. L. Lewis (2010), Present-day and future contributions of glacier runoff to summertime flows in a Pacific Northwest watershed: Implications for water resources, *Water Resour. Res.*, *46*, W12509, doi:10.1029/2009WR008968.
- NSRDB (1992), National Solar Radiation Database 1961–1990 User's Manual, Natl. Renew. Energy Lab. Gold. CO 1.
- O'Neel, S., E. Hood, A. Arendt, and L. Sass (2014), Assessing streamflow sensitivity to variations in glacier mass balance, *Clim. Change*, *123*, 329–341.
- Oerlemans, J. (1992), Climate sensitivity of glaciers in southern Norway: Application of an energy-balance model to Nigardsbreen, Hellstugubreen and Alftobreen, *J. Glaciol.*, *38*, 223–232.
- Oerlemans, J., R. H. Giesen, and M. R. Van Den Broeke (2009), Retreating alpine glaciers: Increased melt rates due to accumulation of dust (Vadret da Morteratsch, Switzerland), *J. Glaciol.*, *55*, 729–736.
- Oke, T. R. (1987), *Boundary Layer Climates*, Methuen, London.
- Ostenso, N. A., P. V. Sellmann, and T. L. Péwé (1965), The bottom topography of Gulkana Glacier, Alaska Range, Alaska, *J. Glaciol.*, *5*, 651–660.
- Patric, J. H., and P. E. Black (1968), *Potential Evapotranspiration and Climate in Alaska by Thornthwaite's Classification*, Pacific Northwest Forest and Range Experiment Station, U.S. Dept. of Agriculture, Juneau, Alaska.
- Pellicciotti, F., M. Carenzo, J. Helbing, S. Rimkus, and P. Burlando (2009), On the role of subsurface heat conduction in glacier energy-balance modelling, *Ann. Glaciol.*, *50*, 16–24.

- Radić, V., and R. Hock (2014), Glaciers in the Earth's hydrological cycle: Assessments of glacier mass and runoff changes on global and regional scales, in *The Earth's Hydrological Cycle*, edited by L. Bengtsson et al., pp. 813–837, Springer, Netherlands.
- Ragetti, S., and F. Pellicciotti (2012), Calibration of a physically based, spatially distributed hydrological model in a glacierized basin: On the use of knowledge from glaciometeorological processes to constrain model parameters, *Water Resour. Res.*, *48*, W03509, doi:10.1029/2011WR010559.
- Raper, S. C. B., and R. J. Braithwaite (2009), Glacier volume response time and its links to climate and topography based on a conceptual model of glacier hypsometry, *Cryosphere*, *3*, 183–194.
- Reusser, D. E., W. Buytaert, and E. Zehe (2011), Temporal dynamics of model parameter sensitivity for computationally expensive models with the Fourier amplitude sensitivity test, *Water Resour. Res.*, *47*, W07551, doi:10.1029/2010WR009947.
- Richter, B. D., J. V. Baumgartner, J. Powell, and D. P. Braun (1996), A method for assessing hydrologic alteration within ecosystems, *Conserv. Biol.*, *10*, 1163–1174.
- Royer, T. C. (1982), Coastal fresh water discharge in the northeast Pacific, *J. Geophys. Res.*, *87*, 2017–2021, doi:10.1029/JC087iC03p02017.
- Rutt, I. C., M. Haggorn, N. R. J. Hulton, and A. J. Payne (2009), The Glimmer community ice sheet model, *J. Geophys. Res.*, *114*, F02004, doi:10.1029/2008JF001015.
- Salamatin, A. N., and A. B. Mazo (1985), Formulation and study of the problem of recovering the bed of a glacier from the profile of its surface, *Mater. Glyatsiol. Issled.*, *52*, 99–104.
- Shea, J. M., W. W. Immerzeel, P. Wagnon, C. Vincent, and S. Bajracharya (2015), Modelling glacier change in the Everest region, Nepal Himalaya, *Cryosphere*, *9*, 1105–1128.
- Stenborg, T. (1965), Problems concerning winter run-off from glaciers, *Geogr. Ann. Ser. Phys. Geogr.*, *47*, 141–184.
- Thompson, E. S. (1976), Computation of solar radiation from sky cover, *Water Resour. Res.*, *12*, 859–865, doi:10.1029/WR012i005p00859.
- Van Beusekom, A. E., S. R. O'Neel, R. S. March, L. C. Sass, and L. H. Cox (2010), Re-analysis of Alaskan benchmark glacier mass-balance data using the index method. US Geol. Surv. Sci. Investig. Rep. 5247, 16. URL. [Available at <http://pubs.usgs.gov/sir/2010/5247/pdf/sir20105247.pdf>.]
- Van de Wal, R. S. W., and M. Wild (2001), Modelling the response of glaciers to climate change by applying volume-area scaling in combination with a high resolution GCM, *Clim. Dyn.*, *18*, 359–366.
- Wang, J., M. Jin, D. L. Musgrave, and M. Ikeda (2004), A hydrological digital elevation model for freshwater discharge into the Gulf of Alaska, *J. Geophys. Res.*, *109*, C07009, doi:10.1029/2002JC001430.
- Ward-Garrison, C., S. L. Markstrom, and L. E. Hay (2009), Downsizer—A graphical user interface-based application for browsing, acquiring, and formatting time-series data for hydrologic modeling. U.S. Geological Survey Open-File Report 2009-1166:27 URL. [Available at <http://pubs.usgs.gov/of/2009/1166/pdf/OF09-1166.pdf>.]